ACS APPLIED MATERIALS & INTERFACES

Research Article

www.acsami.org

Role of Carbon Nanotube Interlayer in Enhancing the Electron Field Emission Behavior of Ultrananocrystalline Diamond Coated Si-Tip Arrays

Ting-Hsun Chang,[†] Srinivasu Kunuku,[§] Joji Kurian,[‡] Afsal Manekkathodi,[†] Lih-Juann Chen,[†] Keh-Chyang Leou,[§] Nyan-Hwa Tai,*[,†] and I-Nan Lin*[,‡]

[†]Department of Materials Science and Engineering, National Tsing-Hua University, Hsinchu 300, Taiwan, R.O.C

[§]Department of Engineering and System Science, National Tsing-Hua University, Hsinchu 300, Taiwan, R.O.C

[‡]Department of Physics, Tamkang University, Tamsui 251, Taiwan, R.O.C

Supporting Information

ABSTRACT: We improved the electron field emission properties of ultrananocrystalline diamond (UNCD) films grown on Si-tip arrays by using the carbon nanotubes (CNTs) as interlayer and post-treating the films in $CH_4/Ar/H_2$ plasma. The use of CNTs interlayer effectively suppresses the presence of amorphous carbon in the diamond-to-Si interface that enhances the transport of electrons from Si, across the interface, to diamond. The post-treatment process results in hybrid-granular-structured diamond (HiD) films via the induction of the coalescence of the ultrasmall grains in these films that enhanced the conductivity of the films. All these factors contribute toward the enhancement of the electron field emission (EFE) process for the $HiD_{CNT/Si\text{-}tip}$ emitters, with low turn-on field of E_0 = 2.98 V/μm and a large current density of 1.68 mA/cm^2 at an applied field of 5.0 V/μm. The EFE lifetime stability under an operation current of 6.5 μA was improved substantially to $\tau_{HiD/CNT/Si\text{-}tip}$ = 365 min. Interestingly, these $HiD_{CNT/Si\text{-}tip}$ materials also show enhanced plasma illumination behavior, as well as improved robustness against plasma ion bombardment when they are used as the cathode for microplasma devices. The study concludes that the use of CNT interlayers not only increase the potential of these materials as good EFE emitters, but also prove themselves to be good microplasma devices with improved performance.

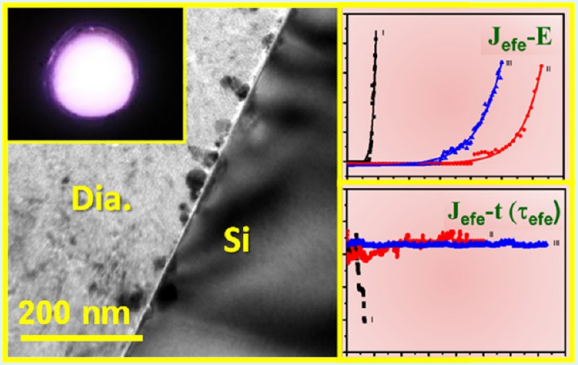

KEYWORDS: *ultrananocrystalline diamond films, hybrid granular structured diamond films, carbon nanotubes, plasma illumination behavior, electron field emission properties*

1. INTRODUCTION

The excellent physiochemical properties of diamond, which contribute toward their high electrical breakdown field and high thermal conductivity, ensures their utility as high temperature or high power devices.[1−5] Ultrananocrystalline diamond (UNCD) films grown in CH_4/Ar plasma contain ultrasmall diamond grains (≤5 nm) interspersed with thick grain boundaries ensuing good conductivity.[6−8] The better transport of electrons through the grain boundaries of UNCD films in comparison with that in microcrystalline diamond (MCD) guarantees the superior electron field emission (EFE) properties of UNCD films.[9,10] A very common approach for improving the EFE properties of diamond films is to increase the field enhancement factor of the emission sited by using silicon nanotips (Si-tips) as templates for growing the diamond films.[11] But care needs to be taken as a possible, electrically resistive a-C thin layer can grow at the diamond-Si interface hindering electron transport across the diamond-Si interface and degrading the EFE properties of the diamond/Si-tip emitters.[11] This clearly implies that the improvement of the diamond-to-Si interfacial characteristics can better the EFE properties of diamond coated Si-emitters. Use of an interfacial material like Au, which can suppress the contribution of the resistive a-C layer, has been reported to be an efficient means to enhance the EFE properties.[12,13] However, the Au material is dissimilar to the Si and diamond materials that might induce some interaction, which is detrimental to the electron transport. The carbon based materials will be more compatible with the diamond and is expected to serve better as interlayer to enhance the interfacial transport behavior for the diamond/Si system. Moreover, the conductivity of the amorphous carbon (a-C) phase located in the grain boundaries of the UNCD films is not sufficiently good, limiting the attainable EFE properties. A post-treatment process which can convert the a-C phase into

Received: January 28, 2015
Accepted: March 20, 2015
Published: March 20, 2015

DOI: 10.1021/acsami.5b00844
ACS Appl. Mater. Interfaces 2015, 7, 7732−7740

more conducting graphitic phase can possibly improve the EFE properties of UNCD films.

In this present study, we enhanced the electron transport behavior across the diamond-to-Si interface, by utilizing carbon nanotubes (CNTs) as the interlayer. Moreover, we improved the conductivity of the UNCD films via the post-treatment in a $CH_4/H_2/Ar$ plasma to form hybrid granular structure diamond (HiD) films. On Si-tip array templates, which contains CNTs as interlayer, these HiD films are grown and enhanced EFE performance for the HiD/Si-tip emitters are obtained that sheds light upon the mechanism by which the EFE behavior gets enhanced.

2. EXPERIMENTAL SECTION

The Si-tip arrays were first fabricated by a process schematically shown in Figure 1. First, 8 μm × 8 μm squares were patterned on the photoresist (PR, EPG512, 1 μm), which was spin-coated on a Si substrate, using the standard photolithography process. The process was followed by reactive ion etching using SF_6(20%) + O_2(80%) gas with 20 Pa chamber pressure and 70 W Radio Frequency power for 15 min (step 1). The residual PR was removed using acetone to form Si-tip arrays. A thin Fe layer (10 nm) was coated on Si-tip arrays by a DC sputtering process followed by rapid thermal treatment annealed at 750 °C for 5 min in Ar gas to form Fe catalysts (step 2). The CNTs were grown on Si-tip arrays by a chemical vapor deposition process, in which the temperature was rapidly increased from room temperature to 750 °C within 20 s and hold for 10 min. In the deposition process, C_2H_2 with a flow rate of 70 sccm was used as carbon source and 10% H_2/Ar with a flow rate of 30 sccm was adopted as buffer gas. The carbon source and the buffer gas were separately channeled into the chamber which was maintained at a low pressure of 10 Torr (step 3). The templates thus formed are designated as CNT/Si-tip. Prior to the growth of the diamond films, the CNT/Si-tip were precoated with a thin Au layer (10 nm) by a DC sputtering system, followed by the decoration of nanosized diamond particulates, which is described in detail elsewhere.[14] Very concisely, the CNT/Si-tip were biased at +20 V with respect to the Pt reference electrode in an aqueous solution, containing single digit sized diamond particulates (Plasma Chem) with concentration of 0.1 g/L, for 30 s.

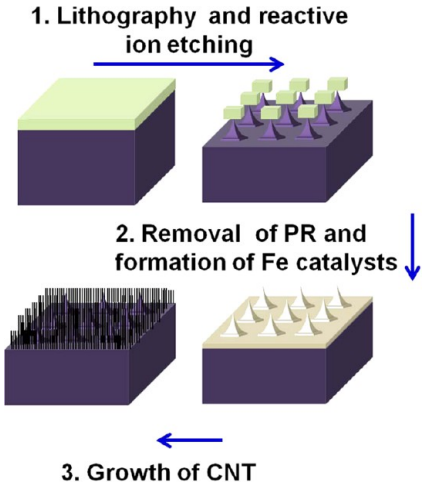

Figure 1. Schematic diagram for the fabrication of CNT/Si-tip array emitters: (1) patterning the PR (1 μm) on Si substrate by the photolithographic and the reactive ion etching processes; (2) striping the PR and sputtering coating the Fe (10 nm) followed by annealing at 750 °C for 5 min; and (3) growth of CNTs by thermal CVD process (C_2H_2, 750 °C, 10 min).

The UNCD films were grown on the nanodiamond decorated CNT/Si-tip by using microwave plasma enhanced chemical vapor deposition system (2.45 GHz, IPLAS-CYRANNUS) in a CH_4 (1%)/Ar plasma with a microwave power of 1200 W for 60 min. The pressure and the total flow rate were maintained at 120 Torr and 100 sccm, respectively. No external heater was used to heat the substrate. The substrate temperature rised to around 450 °C because of the plasma bombardment heating. This was monitored by a thermocouple embedded in the stainless steel substrate holder. The samples were designated as $UNCD_{CNT/Si\text{-}tip}$. Notably, the decoration of the nanosized diamond particulates on CNTs is necessary, as the bare CNTs grown on Si-tip arrays will be etched away completely by the CH_4/Ar plasma used for growing UNCD films; the decoration process facilitates the nucleation of UNCD diamond on CNTs. It has been demonstrated that nanosized diamond particulates is resistant to plasma ion bombardment and can be used as a mask for patterning the diamond nanostructure in RIE process.[15] Moreover, in our previous studies,[14] we observed that coating a thin layer of nanodiamond particulates on Si can effectively suppress the formation of a-C, implying that the presence of nanodiamond particulates can promote the nucleation of diamond films (Figure S1). Therefore, it is expected that the presence of nanodiamond particulates can not only protect the CNTs from plasma bombardment etching but also facilitate the nucleation of diamond. Subsequently, the $UNCD_{CNT/Si\text{-}tip}$ was post-treated in a CH_4/H_2(50%)/Ar(49%) plasma with 80 Torr chamber pressure and 1300 W microwave power for 60 min. This resulted in HiD films. The obtained samples were designated as $HiD_{CNT/Si\text{-}tip}$.

The morphology, bonding structure and the microstructure of the bare CNT/Si-tip, $UNCD_{CNT/Si\text{-}tip}$ or $HiD_{CNT/Si\text{-}tip}$ were examined employing scanning electron microscopy (SEM) (JEOL-6500), UV-Raman spectroscopy (Lab Raman HR800, Jobin Yvon, λ = 325 nm) and transmission electron microscopy (TEM; JEOL-2100F operated at 200 kV), respectively. The EFE properties of these emitters were measured using a tunable parallel plate setup, in which the cathode used was the diamond coated emitters and the anode was a molybdenum rod with a diameter of 2.0 mm. The cathode-to-anode distance was controlled using a micrometer. The current−voltage (I−V) characteristics were measured using an electrometer (Keithley 2410) under pressure below 10^{-6} Torr. The results were modeled by Fowler−Nordheim theory.[16]

The plasma illumination (PI) characteristics of a microplasma device, using bare CNT/Si-tip, $UNCD_{CNT/Si\text{-}tip}$, and $HiD_{CNT/Si\text{-}tip}$ as cathodes, were also investigated. In the microplasma devices, an ITO-coated glass was used as the anode and the cathode-to-anode separation was fixed by a Teflon spacer (1.0 mm in thickness). A circular hole of about 3.0 mm in diameter was cut out from the PTFE spacer to form a microcavity. The plasma was triggered using a pulsed direct current voltage in a bipolar pulse mode (20 ms square pulse, 6 kHz repetition rate). The microplasma devices were placed in a glass chamber, which was evacuated to a base pressure of 0.1 mTorr and was then purged with Ar for 10 min. Argon gas was channeled into the chamber at a flow rate of 10 sccm and the chamber pressure was maintained at 2 Torr throughout the measurements. The plasma current versus applied voltage was measured using an electrometer (Keithley 237).

3. RESULTS AND DISCUSSION

(a). Effect of Diamond Coating on the EFE Properties of CNT/Si-tip Emitters. Figure 2a and b show the SEM morphology of as prepared and CNT/Si-tip emitters, respectively, with the insets revealing the enlarged micrographs of the emitter. The CNT/Si-tip emitters possess desireable EFE properties, inferred from the J_{efe}−E curves in Figure 3a (curve I) and the associated Fowler−Nordheim plots in Figure 3b (curve I). The EFE process of the CNT/Si-tip can be turned on at $(E_0)_{CNT/Si\text{-}tip}$ = 0.64 V/μm and the EFE current density reaches a large value of $(J_e)_{CNT/Si\text{-}tip}$ = 2.07 mA/cm^2 at an applied field of 0.93 V/μm. These EFE parameters are better than that of CNTs grown directly on planar Si substrates,[17] which have slightly larger turn-on field of $(E_0)_{CNT/Si}$ =0.73 V/μm and lower

DOI: 10.1021/acsami.5b00844
ACS Appl. Mater. Interfaces 2015, 7, 7732−7740

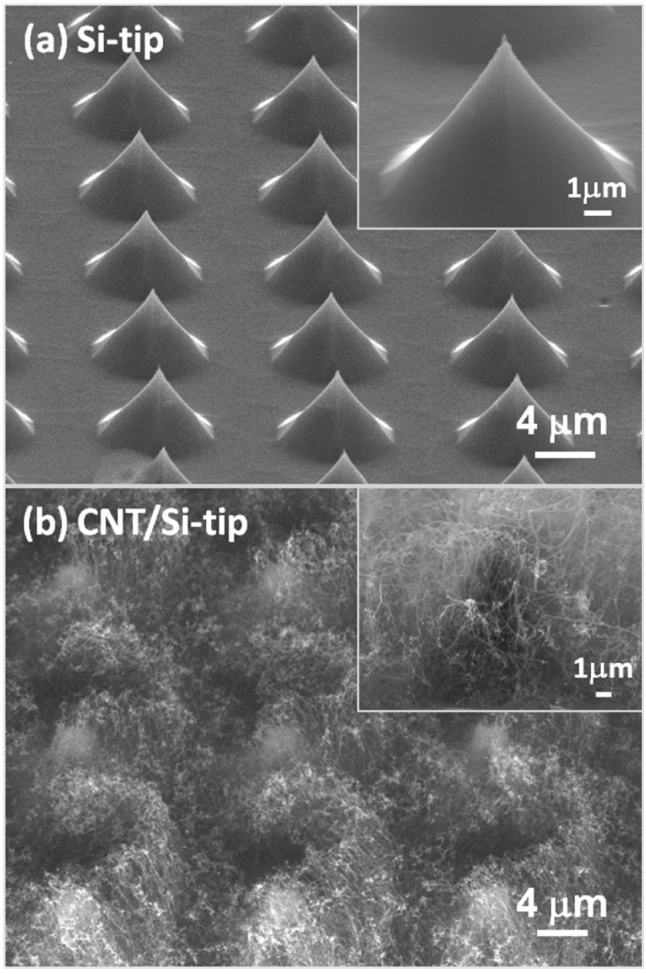

Figure 2. SEM micrographs of (a) the Si-tip arrays and (b) the CNTs grown on Si-tip arrays. The insets in panels a and b are the enlarged SEM micrograph of a single Si-tip or a CNT/Si-tip, respectively.

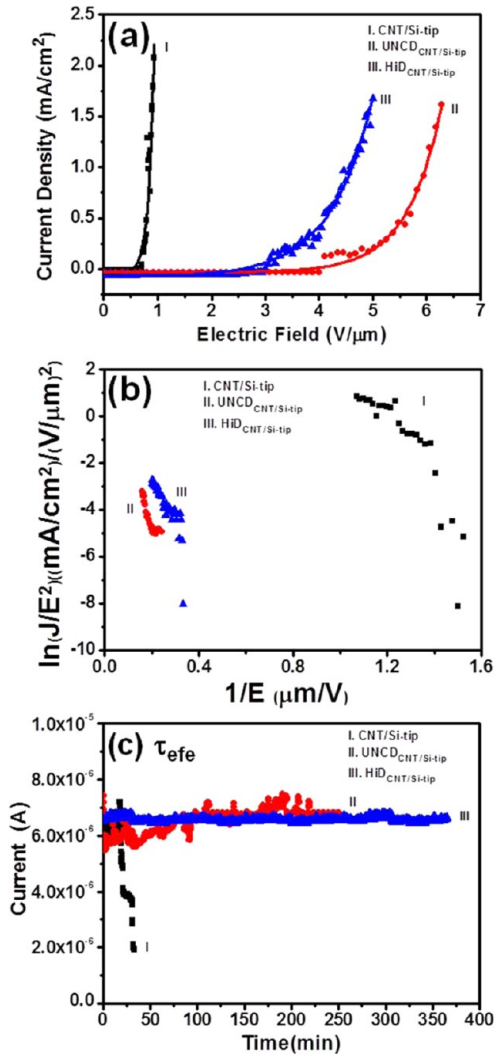

Figure 3. Electron field emission properties (a) J_e–E curves, (b) the corresponding Fowler–Nordhiem plots, ln (J_e/E^2) vs 1/E curve, and (c) the lifetime test at 6.5 μA (0.18 mA/cm^2) of (I) CNT/Si-tip, (II) $UNCD_{CNT/Si-tip}$, and (III) $HiD_{CNT/Si-tip}$ emitters.

EFE current density of $(J_e)_{CNT/Si}$ = 1.1 mA/cm^2 at an applied field of 1.05 V/μm.

Panel I in Figure 4 shows that the microplasma devices using CNT/Si-tip as cathode can be ignited at a low voltage of 360 V, which corresponds to a threshold field of $(E_{pl})_{CNT/Si-tip}$ = 3600 V/cm. The brightness of the PI images increases monotonically with the applied voltage. The performance of the microplasma devices is better illustrated as the plasma current density-applied field (J_{pl}–E) curves in Figure 5a. Curve I in this figure indicates that the J_{pl} increases from $(J_{pl})_{CNT/Si-tip}$ = 0.69 mA/cm^2 at an applied field of 3600 V/cm to around 2.01 mA/cm^2 at 5600 V/cm. From each (J_{pl}) value, the plasma density, which is also known as the electron density (n_e) for the plasma, is calculated. The proceedures for calculating the plasma density of the microplasma devices from the plasma current density is detailed elsewhere.[18] Curve I in Figure 5b shows that the n_e of the CNT/Si-tip-based microplasma devices increase monotonously against the applied field from $(n_e)_{CNT/Si-tip}$ = 0.75 × 10^{14} cm^{-3} at an applied field of 3600 V/cm to a value of $(n_e)_{CNT/Si-tip}$ = 1.46 × 10^{14} cm^{-3} at an applied field of 5600 V/cm.

Apart from the extremely good EFE properties exhibited by the CNT/Si-tip emitters, microplasma devices using these materials as cathode exhibit superb PI behavior. But the downside is that they have a short lifetime. Curve I in Figure 3c shows that the EFE lifetime of CNT emitters is as short as 28 min when tested under 6.5 μA at 10^{-6} Torr pressure, whereas curve I in Figure 5c indicates that the CNT/Si-tip-based microplasma devices can last only for 48 min when tested in a plasma current density of 1.53 mA/cm^2 (Ar, 2 Torr). Apparently, the sp^2-bonded carbons can not withstand either the high temperature induced by the self-heating mechanism during the EFE measurements or the Ar-ion bombardment in the plasma environments during microplasma operation. An EFE material that can survive these harsh environments will surely have the upper hand from an application point of view.

To improve the durability of these electron emitters, coating of a diamond film on top of the CNT/Si-tip emitters is attempted. The decoration of the nanodiamond particulates on CNT/Si-tip can facilitate the nucleation of diamond on CNTs. But when the CH_4-content in the CH_4/Ar plasma is smaller than 4%, the CNTs were still etched out in the microwave plasma leading to the absence of diamond films. When the CH_4-content is larger than this critical value, the UNCD films grow well, fully covering the CNTs. Figure 6a shows the SEM micrograph of CNT/Si-tip after the coating of UNCD films. Moreover, the CH_4(1%)/H_2(50%)/Ar(49%) plasma

DOI: 10.1021/acsami.5b00844
ACS Appl. Mater. Interfaces 2015, 7, 7732–7740

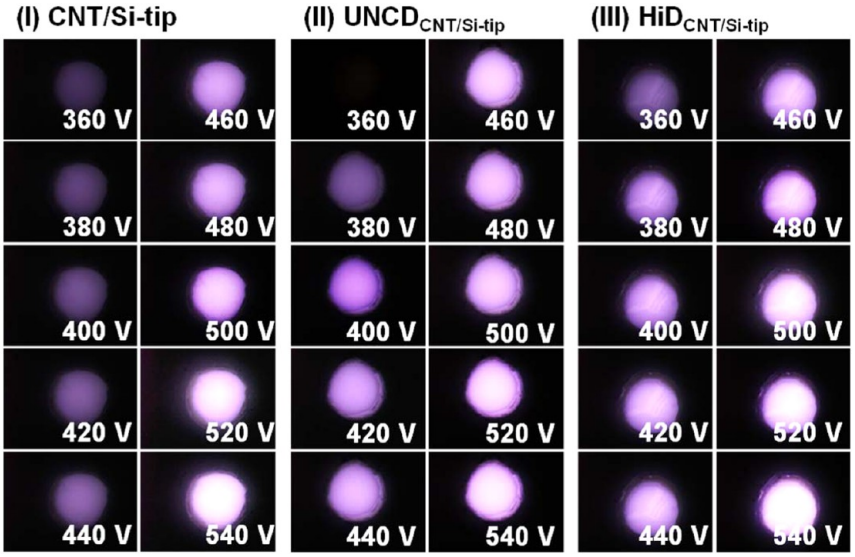

Figure 4. Plasma illumination images of (I) CNT/Si-tip, (II) UNCD$_{CNT/Si-tip}$, and (III) HiD$_{CNT/Si-tip}$-based microplasma devices.

post-treatment process is utilized to modify the granular structure of the UNCD grown on CNT/Si-tip, so as to further improve the characteristics of the EFE emitters. The typical SEM morphology of the HiD$_{CNT/Si-tip}$ is shown in Figure 6b, indicating the formation of cauliflower-like structures with size around 100 nm.The Raman spectroscopic studies reveal that, apart from a single G-band at 1580 cm^{-1} for CNT/Si-tip emitters (curve I, Figure 7), the UV Raman spectra corresponding to these UNCD$_{CNT/Si-tip}$ emitters (curve II, Figure 7) contains several Raman resonance peaks. The D-band resonance peak at 1332 cm^{-1},[19] representing diamond, the D*-band (~1350 cm^{-1}) and G-band (~1580 cm^{-1}),[20,21] representing disordered carbon and the graphitic phase, respectively, and the υ_1-band (1140 cm^{-1}), representing the grain boundary phase, *trans*-polyacetylene,[20,21] are also observed. The broadness of the Raman resonance peaks is presumably owing to the smallness of the diamond grains in the UNCD films. The Raman spectra of HiD$_{CNT/Si-tip}$ are shown in curve III of Figure 7, indicating that these materials also contain D-band, D*-band, G-band and ν_1-band, which are essentially the same as that of UNCD$_{CNT/Si-tip}$, except that the HiD$_{CNT/Si-tip}$ contains a much larger and sharper D-band (1332 cm^{-1}). These results imply that the HiD$_{CNT/Si-tip}$ materials contain some large diamond grains coexisting with ultrasmall diamond grains.

The coating of diamond films on CNT/Si-tip emitters evidently modify the EFE and PI behavior. Curve II in Figure 3a and b show that the EFE process of the UNCD$_{CNT/Si-tip}$ emitters can be turned on at $(E_0)_{UNCD/CNT/Si-tip}$ = 3.95 V/μm, attaining an EFE current density of $(J_e)_{UNCD/CNT/Si-tip}$ = 0.21 mA/cm^2 at an applied field of 5.0 V/μm. The benefit of coating the UNCD films on CNT/Si-tip is the marked improvement in the robustness of the emitters. Curve II in Figure 3c reveals that UNCD$_{CNT/Si-tip}$ emitters tested under 6.5 μA can last more than $\tau_{UNCD/CNT/Si-tip}$ = 251 min without showing any sign of decay in EFE characteristics, compared with the short lifetime of CNT/Si-tip ($\tau_{CNT/Si-tip}$ = 28 min, curve I, Figure 3c).

Usage of HiD films to replace for the UNCD films in the diamond-CNT/Si-tip markedly improves the EFE of the emitters. Curve III in Figures 3a and b show that the EFE process of the HiD$_{CNT/Si-tip}$ emitters can be turned on at $(E_0)_{HiD/CNT/Si-tip}$ = 2.98 V/μm, achieving a EFE current density

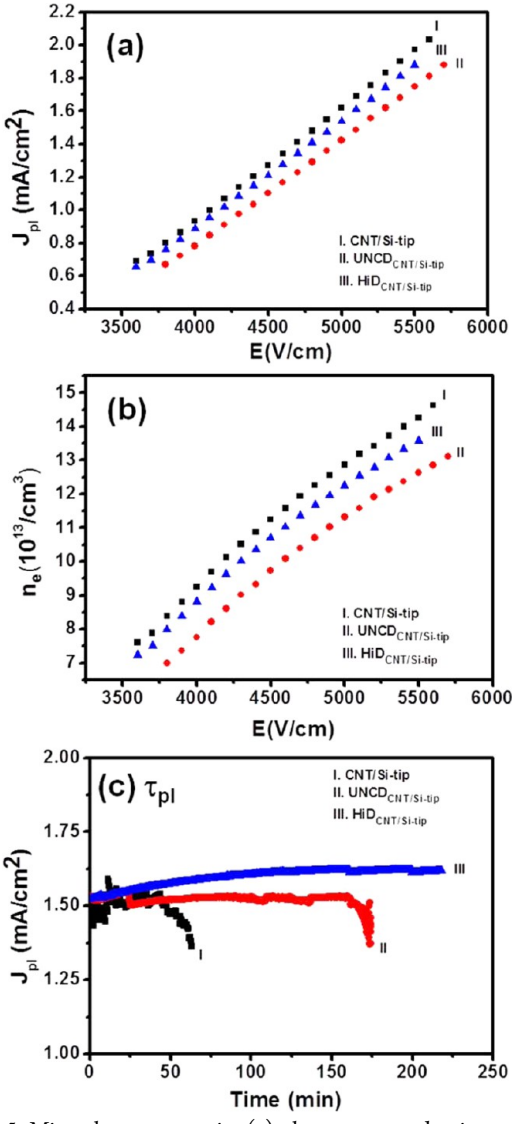

Figure 5. Microplasma properties (a) plasma current density vs applied field (J_{pl}–E), (b) plasma density vs applied field (n_e–E), and (c) plasma lifetime test under 100 μA (1.53 mA/cm^2) for (I) CNT/Si-tip, (II) UNCD$_{CNT/Si-tip}$, and (III) HiD$_{CNT/Si-tip}$-based microplasma devices.

DOI: 10.1021/acsami.5b00844
ACS Appl. Mater. Interfaces 2015, 7, 7732−7740

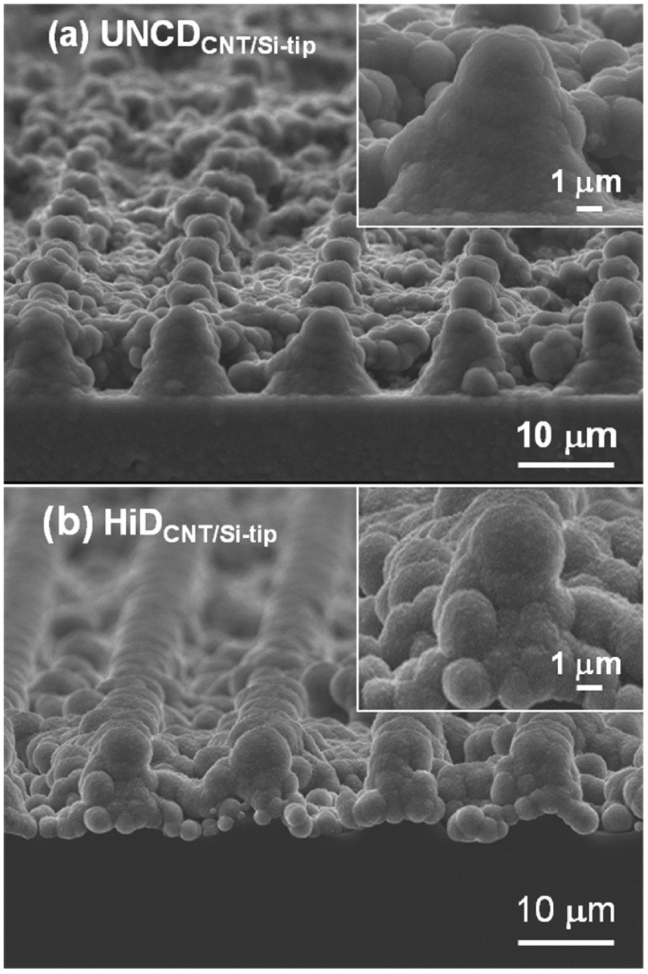

Figure 6. Top-view SEM micrographs of (a) $UNCD_{CNT/Si\text{-}tip}$ and (b) $HiD_{CNT/Si\text{-}tip}$ emitters. The insets show the enlarged SEM micrograph of a single $UNCD_{CNT/Si\text{-}tip}$ and $HiD_{CNT/Si\text{-}tip}$ tip.

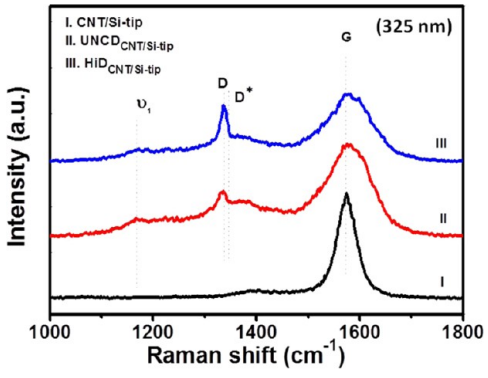

Figure 7. Raman spectra of (I) CNT/Si-tip, (II) $UNCD_{CNT/Si\text{-}tip}$, and (III) $HiD_{CNT/Si\text{-}tip}$ materials.

of $(J_e)_{HiD/CNT/Si\text{-}tip}$ = 1.68 mA/cm^2 at an applied field of 5.0 V/μm. This is better than that of the $UNCD_{CNT/Si\text{-}tip}$ emitters (cf., Table 1). What is intriguing is that, contrary to the phenomenon that materials possessing better EFE properties usually show inferior lifetime stability, converting the UNCD films into HiD ones enhance the EFE properties of the CNT/Si-tip emitters without sacrificing the robustness of the devices. Curve III in Figure 3c shows that the $HiD_{CNT/Si\text{-}tip}$ emitters exhibit longer lifetime of $\tau_{HiD/CNT/Si\text{-}tip}$ = 365 min than the

Table 1. EFE Properties of CNT/Si-Tip Arrays, $UNCD_{CNT/Si\text{-}tip}$, and $HiD_{CNT/Si\text{-}tip}$ Emitters

	electron field emission behavior		
materials	E_0[a] (V/μm)	J_e[b] (mA/cm^2)	τ_{efe}[c] (min)
Si pyramids[11]	21.34	<0.01	
HiD/Si pyramids[11]	5.99	1.10	
CNTs/Si-tip arrays[this study]	0.64	2.07@0.93	28
$UNCD_{CNT/Si\text{-}tip}$[this study]	3.95	0.21@5.0	251
$HiD_{CNT/Si\text{-}tip}$[this study]	2.98	1.68@5.0	365

[a]E_0: The turn-on field for inducing EFE process, which was designated as the interception of the straight line segments extrapolated from the of low-field and high field of FN plots. [b]J_e: The EFE current density at the designated applied field in V/μm. [c]τ_{efe}: The lifetime measured at applied current of 6.5 μA.

Table 2. Plasma Illumination Properties of a Microplasma Device Using CNT/Si-Tip Arrays, $UNCD_{CNT/Si\text{-}tip}$ as Cathode

	plasma illumination behavior			
materials	$(E_{th})_{pl}$[a] (V/cm)	J_{pl}[b] (mA/cm^2)	n_e[c] 10^{14} cm^{-3}	τ_{pl}[d] (min)
CNT/Si-tip arrays	3600	1.97	1.42	48
$UNCD_{CNT/Si\text{-}tip}$	3800	1.75	1.26	174
$HiD_{CNT/Si\text{-}tip}$	3600	1.88	1.36	218

[a]$(E_{th})_{pl}$: The threshold field for igniting the plasma in parallel-plate microplasma devices. [b]J_{pl}: The plasma current density in parallel-plate microplasma devices measured at an applied field of 5500 V/cm. [c]n_e: The plasma density, which is also the electron density in the parallel-plate microplasma devices, measured at an applied field of 5500 V/cm. [d]τ_{pl}: The lifetime measured at 1.53 mA/cm^2 applied current density in parallel-plate microplasma devices.

$UNCD_{CNT/Si\text{-}tip}$ emitters ($\tau_{UNCD/CNT/Si\text{-}tip}$ = 251 min) when tested in 6.5 μA. These EFE behavior are listed in Table 1.

On the other hand, the $UNCD_{CNT/Si\text{-}tip}$-based microplasma devices require slightly larger applied voltage to ignite the plasma, $(E_{pl})_{UNCD/CNT/Si\text{-}tip}$ = 3800 V/cm (panel II, Figure 4) and achieve smaller plasma current density, $(J_{pl})_{UNCD/CNT/Si\text{-}tip}$ = 1.75 mA/cm^2 at 5600 V/cm (curve II, Figure 5a), compared with that of the CNT/Si-tip-based microplasma devices. Similarly, the plasma density, n_e, can be estimated from the corresponding J_{pl}-value. The n_e–E curves of the $UNCD_{CNT/Si\text{-}tip}$-based microplasma devices are shown as curve II in Figure 5b, revealing that the n_e values reach around ~1.26 × 10^{14} cm^{-3} at an applied field of 5500 V/cm. Again, coating UNCD films on CNT/Si-tip significantly improves the lifetime stability of the corresponding microplasma devices. Curve II in Figure 5c depicts that the $UNCD_{CNT/Si\text{-}tip}$-based microplasma devices can be operated at 1.53 mA/cm^2 for more than $(\tau_{pl})_{UNCD/CNT/Si\text{-}tip}$ = 174 min before starting to decay. This is overwhelmingly superior to the CNT/Si-tip-based microplasma devices ($(\tau_{pl})_{UNCD/CNT/Si\text{-}tip}$= 48 min, curve I, Figure 5c).

Panel III in Figure 4 shows that the $HiD_{CNT/Si\text{-}tip}$-based microplasma devices can be ignited at lower threshold field of $(E_{pl})_{HiD/CNT/Si\text{-}tip}$ = 3600 V/cm and exhibit better plasma illumination properties, when compared to the $UNCD_{CNT/Si\text{-}tip}$-based ones. The plasma current density and the plasma density increases monotonously with applied field, attaining a large J_{pl} value as $(J_{pl})_{HiD/CNT/Si\text{-}tip}$ = 1.88 mA/cm^2 (curve III, Figure 5a) and a large n_e value as $(n_e)_{HiD/CNT/Si\text{-}tip}$ = 1.36 × 10^{14} cm^{-3} (curve III, Figure 5b) at an applied field of 5500 V/cm. These PI parameters are listed in Table 2, showing the superiority of

DOI: 10.1021/acsami.5b00844
ACS Appl. Mater. Interfaces 2015, 7, 7732–7740

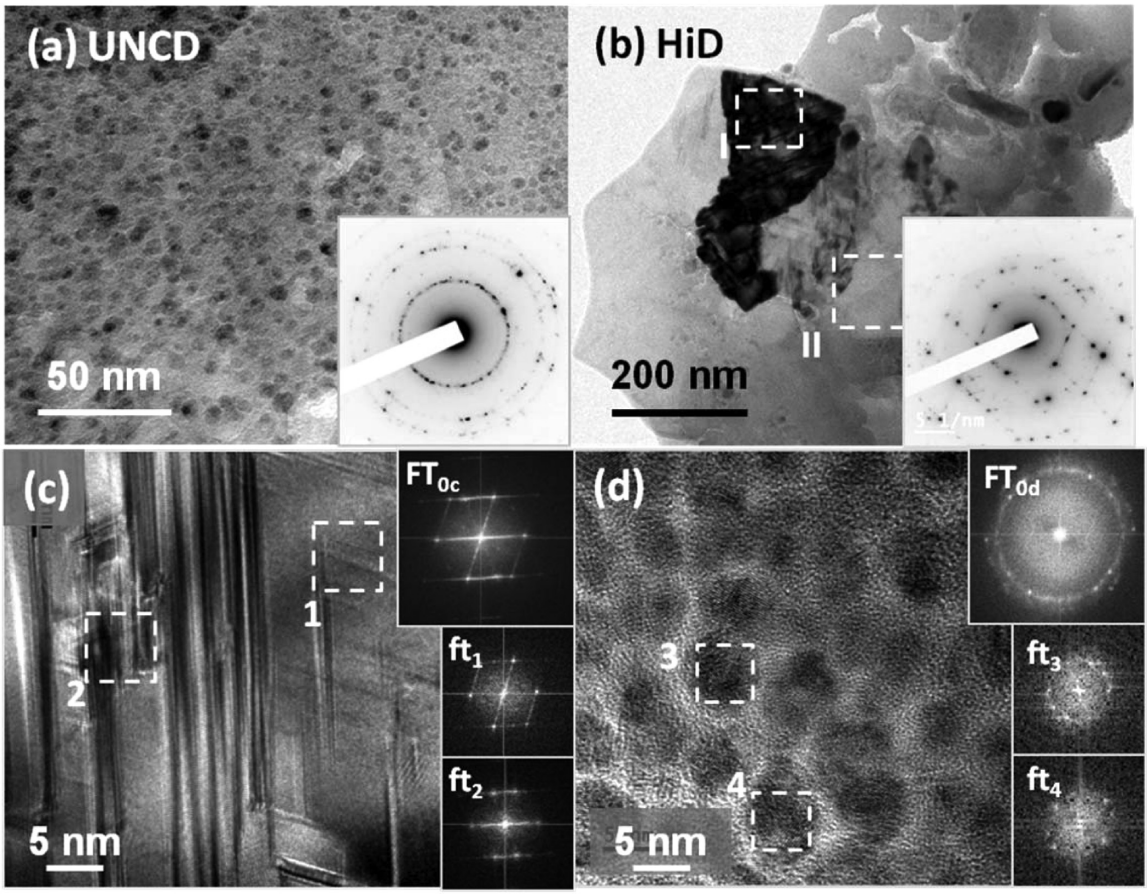

Figure 8. Plan-view bright field (BF) TEM micrographs of (a) the $UNCD_{CNT/Si\text{-}tip}$ materials and (b) the $HiD_{CNT/Si\text{-}tip}$ materials, with the insets showing the corresponding SAED. (c, d) The structure image of the large diamond aggregates (c), which is designated as region I in panel b, and the small diamond area (d), which is designated as II in panel b, of the $HiD_{CNT/Si\text{-}tip}$ materials. In panels c and d, the Fourier-transformed diffractogram of the entire region in structure image was designated as FT_{0c} and FT_{0d}, respectively, whereas those for the areas designated as 1, 2, 3, and 4 were represented by ft_1, ft_2, ft_3, and ft_4 images, respectively.

microplasma devices, using the $HiD_{CNT/Si\text{-}tip}$ as cathode, compared with microplasma devices using $UNCD_{CNT/Si\text{-}tip}$-based ones. Curve III in Figure 5c demonstrates that the microplasma devices using $HiD_{CNT/Si\text{-}tip}$ emitters as cathode can last more than 218 min at 1.53 mA/cm^2 plasma current, which is better than the that of the devices using $UNCD_{CNT/Si\text{-}tip}$ as cathode (174 min, curve II, Figure 5c). Restated, converting the UNCD films coated on CNT/Si-tip into HiD films not only enhance the PI behavior, but also efficiently improves the robustness for the corresponding microplasma devices that is actually of more concern from an applications point of view.

It should be mentioned that the applied field required for igniting the microplasma devices is perceptibly smaller than the turn-on field, for inducing the EFE process of the diamond films used as the cathode. The question then pondered over should be why a cathode material with superior EFE properties results in better plasma illumination performance. In a microplasma device, the plasma is triggered when the secondary electrons emitted from the cathode gain sufficient kinetic energy to ionize the gas molecules (e.g., 15.7 eV for Ar-species). Before the onset of plasma, the electric field imposed on the cathode materials is usually <0.55 V/μm (for a parallel plate microplasma device with 1 mm cathode-to-anode spacing and operated at 550 V) and is far below the turn-on field, E_0, needed for inducing the EFE process ($(E_0)_{EFE}$ = 2.98−3.95 V/μm). Only the secondary electrons contribute toward the triggering of the ionization of Ar-gas molecules for sustaining the plasma. Therefore, it is assessed that the lower EFE turn-on field for $HiD_{CNT/Si\text{-}tip}$ is not helpful in lowering the threshold field for igniting the plasma, when compared with that for $UNCD_{CNT/Si\text{-}tip}$ ones. However, when the plasma is ignited, a plasma sheath is formed in the vicinity of cathode, where the electric field drastically increases. For a typical plasma with the sheath around 10 μm thick, the electric field experienced by the cathode increases to around 35.0−55.0 V/μm for an applied voltage of 350−550 V. Such a field is much larger than that necessary for turning on the EFE process for most of the diamond films. Large number of electrons will be emitted from the diamond cathode that increases the cascading ionization for the Ar gas molecules and also increases the plasma current density. Therefore, larger plasma current density and plasma density are observed when $HiD_{CNT/Si\text{-}tip}$ is used as cathode, using them as replacements for the $UNCD_{CNT/Si\text{-}tip}$ ones (cf., Table 2).

(b). TEM Microstructure. To understand how the $CH_4/H_2/Ar$ post-treatment process and the use of CNTs interlayer enhance the EFE properties of UNCD, the microstructure of these films are examined using TEM. Figures 8a and 8b show, respectively, the plan view TEM micrographs of the UNCD films grown on CNT/Si-tip before and after the $CH_4/H_2/Ar$ plasma post-treatment process, which are the UNCD and HiD films, respectively. The corresponding selected area diffraction

DOI: 10.1021/acsami.5b00844
ACS Appl. Mater. Interfaces 2015, 7, 7732−7740

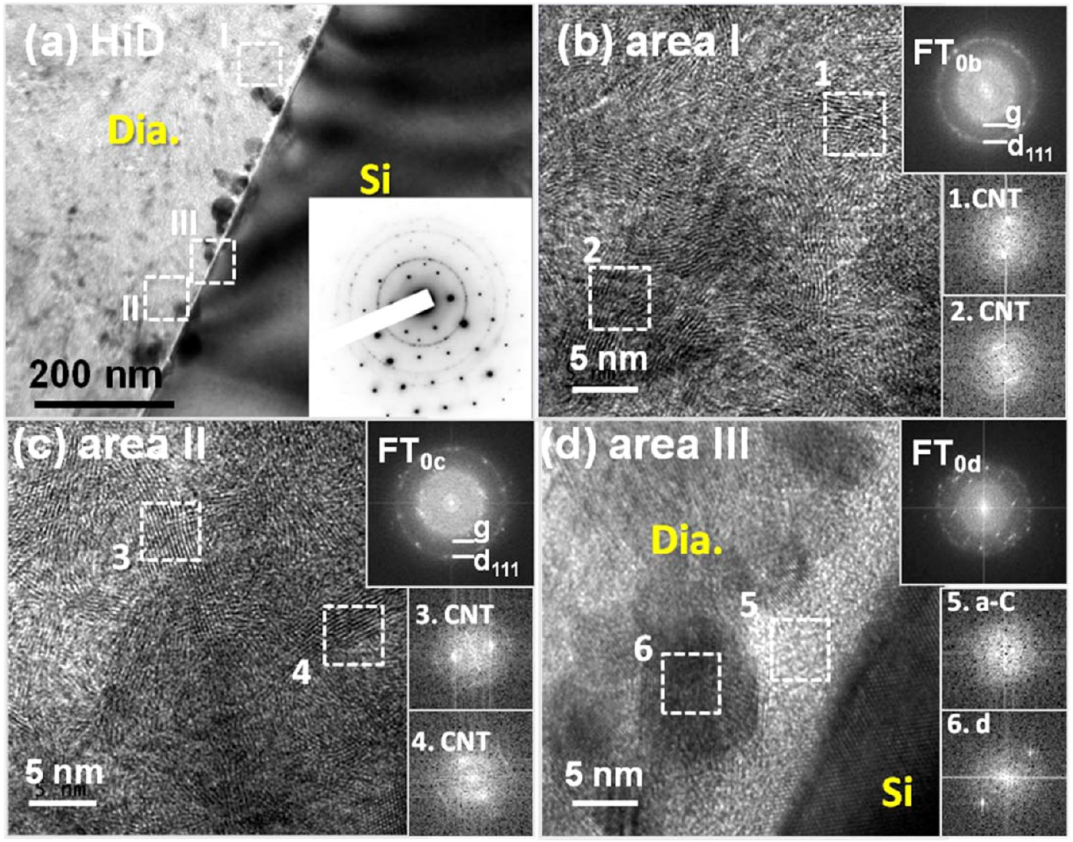

Figure 9. (a) Cross-sectional bright field (BF) TEM micrographs of the $HiD_{CNT/Si\text{-}tip}$ materials and (b–d) the structure image of the regions designated as I–III in panel a, respectively. the Fourier-transformed diffractogram of the entire region in structure images in panels b–d were designated as FT_{0b}, FT_{0c}, and FT_{0d}, respectively, whereas those for the areas designated as 1–6 were represented by ft_1–ft_6 images, respectively.

patterns (SAED) are shown as insets. These figures confirm that the UNCD films contain ultrasmall diamond grains of uniform size (~5 nm, Figure 8a), whereas the HiD films contain large diamond aggregates dispersed in a matrix of ultrasmall grains (Figure 8b). Figure 8c shows the TEM structure image of the central region of the diamond aggregates in HiD films (designated as region I, Figure 8b), depicting that this region contains abundant parallel fringes with irregular spacing. The presence of streaks, the rel-rods, associated with each major diffraction spot is observed in the Fourier-transformed diffractogram corresponding to the entire TEM structure image (FT_{0c}-image) in Figure 8c. These rel-rods lie in a direction perpendicular to the parallel fringes in the structure image. The presence of the parallel fringes and the rel-rods suggest that the diamond aggregates contain abundant planar defects, which are the stacking faults. These, in turn, imply that the formation of the diamond aggregates occurs via coalescence of nanosized diamond grains in UNCD films during the post-treatment process.[22] The presence of stacking faults in these aggregates is highlighted by the ft_1 and ft_2 images associated with the areas 1 and 2 in Figure 8c.

In contrast, Figure 8d shows the TEM structure image corresponding to region II in Figure 8b. That this region consists of ultrasmall diamond grains of uniform size (~5 nm) is clearly viewed from this image. Two of the nanosized diamond grains are highlighted in areas 3 and 4 with the associated FT-image shown in ft_3 and ft_4 of Figure 8d. The FT-image corresponding to entire structure image in Figure 8d is shown as inset FT_{0d}, showing that, besides the ring-shaped diffraction spots corresponding to randomly oriented diamond grains, there exists a large donut-shaped diffuse ring in the center of FT_{0d}-image. Such a diffuse ring proves that this region contains crystalline sp^2-bonded carbon, the nanographitic clusters. Figure 8b–d represent typical granular structure of the bulk regions in HiD films coated on top of CNT/Si-tip, clearly illustrating that the HiD films grown on CNT/Si-tip possess a hybrid granular structure, with a microstructure similar to the one proposed in the literature.[23−25] Presumably, the presence of the nanographitic phase in the HiD films is the prime factor rendering the HiD materials more conductive than the UNCD films, which contain a-C phase along the grain boundaries. Therefore, the $HiD_{CNT/Si\text{-}tip}$ emitters exhibit better EFE properties compared with that of the $UNCD_{CNT/Si\text{-}tip}$ ones.

However, there still remains an unsolved puzzle, namely, why does the HiD films grown on CNT/Si-tip exhibit overwhelmingly superior EFE behavior to the films directly grown on Si-tip arrays ($(E_0)_{HiD/Si\text{-}tip}$ = 5.99 V/μm, $(J_e)_{HiD/Si\text{-}tip}$ = 1.10 mA/cm^2 at 8.5 V/μm applied field).[11] To understand such a phenomenon, the interfacial microstructure of the $HiD_{CNT/Si\text{-}tip}$ emitters is investigated. Figure 9a shows the cross-sectional TEM micrograph of these materials, indicating that the film-to-Si interface is quite sharp. The presence of CNTs is established from Figure 9b and c, which show the detailed microstructure of the two examples designated in Figure 9a, revealing the presence of abundant curved fringes, which are the multiwall CNTs (~10 layers). The FT images, ft_1-ft_4, which correspond to areas 1–4 in these figures, highlight such kind of characteristics. Although the presence of diamond clusters cannot be clearly resolved in these structure images, the co-existence of the diamond clusters with the CNTs is clearly

DOI: 10.1021/acsami.5b00844
ACS Appl. Mater. Interfaces 2015, 7, 7732–7740

ascertained by the presence of the diffraction spots, which are arranged in a ring, in FT_{0b} and FT_{0c} images. Whether the diamond clusters are the newly nucleated one or the nanodiamond particulates decorated on CNTs by electrophoresis cannot be distinctly decided. However, in some areas, the CNTs are preferentially etched away by the plasma, exposing the bare Si surface. In such cases, the diamond clusters can be formed only after the formation of an a-C layer of sufficient thickness. Such a phenomenon is illustrated in Figure 9d corresponding to region III in Figure 9a, in which the presence of the a-C layer is highlighted in area 5 and ft_5-image and the nanodiamond clusters are highlighted in area 6 and ft_6-image in Figure 9d. Nevertheless, the formation of the a-C layer, which usually occurrs when the diamond films are grown directly on Si surface,[14] is effectively circumvented.

The local bonding characteristics of these films are further explored using electron energy loss spectroscopy (EELS). Figure 10a and b indicate, respectively, the core-loss and plasmon-loss EELS spectra corresponding to the bulk region (Figure 8b) and the interface region (Figure 9a) of the $HiD_{CNT/Si\text{-}tip}$ materials. The core-loss EELS spectra depicted as curve I in Figure 10a indicates that the bulk region contains an abrupt rise in the σ^*-band (near 289.5 eV) and a large valley near 302 eV,[26,27] implying that this region is dominantly diamond. The small hump corresponding to the π^*-band at 284.5 eV in the core-loss EEL spectra for $HiD_{CNT/Si\text{-}tip}$ materials indicates the presence of sp^2-bonded carbon, which is presumably residing in the grain boundary regions in these materials. Moreover, the plasmon-loss EELS shown as curve I in Figure 10b reveals a peak at 33 eV (ω_{d2}-band) with a shoulder at 23 eV (ω_{d1}-band). The plasmon-loss EELS is the most effective study to differentiate diamond (sp^3-bonded carbons) from sp^2-bonded carbons and to differentiate crystalline sp^2-bonded carbons (the graphite) from the amorphous ones. The plasmon-loss EEL spectra of the crystalline sp^3-bonded carbons, the diamond phase, show a peak corresponding to the bulk plasmon loss at ω_{d2}-band (33 eV) with a shoulder corresponding to the surface plasmon loss at ω_{d1}-band (23 eV). The ω_{d1}/ω_{d2} ratio is about $1:\sqrt{2}$.[27,28] The graphitic phase shows a prominent peak at ω_{d3}-band (27 eV) and the *a*-C phase shows a peak at ω_{d1}-band (22 eV).[27,28] The plasmon-loss EELS shown as curve I in Figure 10b confirms, again, that the region viewed in Figure 8b is predominantly diamond.

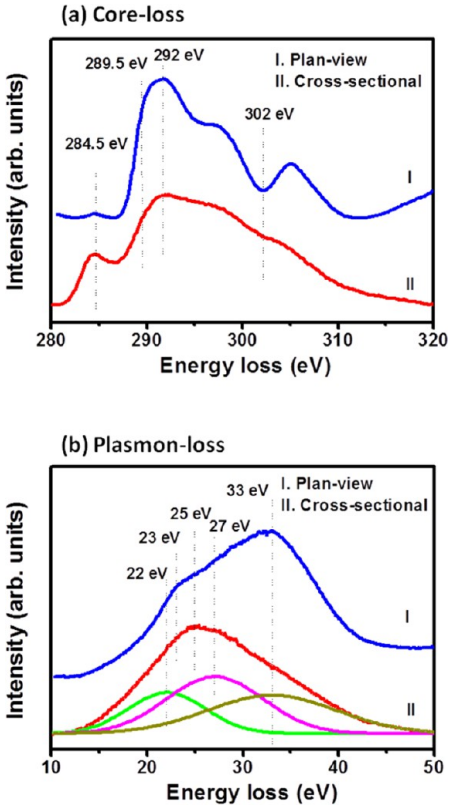

Figure 10. EELS spectra of (a) core-loss and (b) plasmon-loss corresponding to bulk and interfacial regions, respectively, of the $HiD_{CNT/Si\text{-}tip}$ materials. Curve I corresponds to bright field TEM image of bulk region, as shown in Figure 8b, and curve II corresponds to the cross-sectional TEM image, as depicted in Figure 9a.

In contrast, the core-loss EELS spectrum shown as curve II in Figure 10a comprises of a diffuse peak near 290 eV and a large π^*-band at 284.5 eV. There is no signature of sp^3-bonded carbon, that is, the σ^*-band and the deep-valley. Moreover, the plasmon-loss EELS spectrum shown as curve II in Figure 10b consists of only one large diffuse peak near 25 eV, which can be deconvoluted into ω_a-band at 22 eV representing the a-C phase and the ω_g-band at 27 eV representing the graphitic phase with small proportion of ω_{d2}-band at 33 eV (dotted curves, Figure 10b). This is contrary to the phenomenon that the plamon loss EELS of bulk region (curve I, Figure 10b) mainly consists of ω_{d1} (23 eV) and ω_{d2} (33 eV) bands, the diamond phase. Restated, both the core-loss and plasmon-loss EELS shown as curve I in Figure 10a and b substantiates that the bulk region of $HiD_{CNT/Si\text{-}tip}$ materials is diamond, whereas these EELS spectra shown as curve II clearly reveal that the materials in the vicinity of the interface regions are predominantly the sp^2-bonded carbon phase, which is a mixture of the a-C and the graphitic phases. The EELS spectra observed in Figure 10a and b is in accord with the microstructural observation illustrated in TEM micrographs (cf., Figures 8b and 9a). The utilization of CNTs as interlayer effectively suppresses the formation of an a-C resistive layer at the diamond-to-Si interface, facilitating the transport of electrons across the interface. Such an effect, in conjunction with the formation of interconnected nanographitic clusters in the postdeposition-treated UNCD films, results in higher conductivity and thus superior EFE properties of the $HiD_{CNT/Si\text{-}tip}$ materials.

4. CONCLUSIONS

In conclusion, we demonstrate an easy method of synthesizing HiD films on CNT/Si-tip with long lifetime stability of EFE and PI performances, overcoming the poor stability problems of CNTs/Si-tip devices. The $HiD_{CNT/Si\text{-}tip}$ emitters exhibit excellent EFE lifetime stability of τ_{efe} = 365 min, when it is tested at an applied current density of 6.5 μA, compared with short lifetime of CNT/Si-tip emitters (τ_{efe} = 28 min for CNT emittes). In addition, the plasma current density of 1.53 mA/cm^2 is upheld for a period over 218 min, showing better plasma stability for $HiD_{CNT/Si\text{-}tip}$-based microplasma devices, compared with that of bare CNT/Si-tip-based ones (τ_{pl} = 48 min). The present approach of synthesizing HiD films on Si-tip using CNT as interlayer is a direct and simple process that provides a solution for the fabrication of functional field emission devices, and opens new prospects of high definition flat panel displays or microplasma-based devices.

DOI: 10.1021/acsami.5b00844
ACS Appl. Mater. Interfaces 2015, 7, 7732−7740

■ ASSOCIATED CONTENT

Supporting Information

HRTEM and FT images of an interfacial layer between UNCD and Si. This material is available free of charge via the Internet at http://pubs.acs.org.

■ AUTHOR INFORMATION

Corresponding Authors

*E-mail: nhtai@mx.nthu.edu.tw.

*E-mail: inanlin@mail.tku.edu.tw.

Notes

The authors declare no competing financial interest.

■ ACKNOWLEDGMENTS

The authors would like to thank the Ministry of Science and Technology, Taiwan, Republic of China, for the support of this research through the project no. MOST 103-2112-M-032-002 and National Science Council, Taiwan, Republic of China, for the support of this research through the project No. and NSC 101-2221-E-007-064-MY3.

■ REFERENCES

(1) Okano, K.; Koizumi, S.; Silva, S. R. P.; Amaratunga, G. A. J. Low-Threshold Cold Cathodes Made of Nitrogen-Doped Chemical-Vapour-Deposited Diamond. *Nature* **1996**, *381*, 140−141.

(2) Zhu, W.; Kochanski, G. P.; Jin, S.; Seibles, L. Defect-Enhanced Electron Field Emission from Chemical Vapor-Deposited Diamond. *J. Appl. Phys.* **1995**, *78*, 2707−2711.

(3) Yamaguchi, H.; Masuzawa, T.; Nozue, S.; Kudo, Y.; Saito, I.; Koe, J.; Kudo, M.; Yamada, T.; Takakuwa, Y.; Okano, K. Electron Emission from Conduction Band of Diamond with Negative Electron Affinity. *Phys. Rev. B* **2009**, *80*, No. 165321.

(4) Sowers, A. T.; Ward, B. L.; English, S. L.; Nemanich, R. J. Field Emission Properties of Nitrogen-Doped Diamond Film. *J. Appl. Phys.* **1999**, *86*, 3973−3982.

(5) Jiao, S.; Sumant, A.; Kirk, M. A.; Gruen, D. M.; Krauss, A. R.; Auciello, O. Microstructure of Ultrananocrystalline Diamond Films Grown by Microwave Ar−CH_4 Plasma Chemical Vapor Deposition with or without added H_2. *J. Appl. Phys.* **2001**, *90*, 118−122.

(6) Birrell, J.; Gerbi, J. E.; Auciello, O.; Gibson, J. M.; Gruen, D. M.; Carlisle, J. A. Bonding Structure in Nitrogen Doped Ultrananocrystalline Diamond. *J. Appl. Phys.* **2003**, *93*, 5606−5612.

(7) Corrigan, T. D.; Gruen, D. M.; Krauss, A. R.; Zapol, P.; Chang, R. P. H. The Effect of Nitrogen Addition to Ar/CH_4 Plasmas on the Growth, Morphology and Field Emission of Ultrananocrystalline Diamond. *Diamond Relat. Mater.* **2002**, *11*, 43−48.

(8) Zhou, D.; Krauss, A. R.; Qin, L. C.; McCauley, T. G.; Gruen, D. M.; Corrigan, T. D.; Chan, R. P. H.; Gnaser, H. Synthesis and Electron Field Emission of Nanocrystalline Diamond Thin Films Grown from N_2/CH_4 Microwave Plasmas. *J. Appl. Phys.* **1997**, *82*, 4546−4550.

(9) Krauss, A. R.; Auciello, O.; Ding, M. Q.; Gruen, D. M.; Huang, Y.; Zhirnov, V. V.; Givargizov, E. I.; Breskin, A.; Chechen, R.; Shefer, E.; Konov, V.; Pimenov, S.; Karabutov, A.; Rakhimov, A.; Suetin, N. Electron Field Emission for Ultrananocrystalline Diamond Films. *J. Appl. Phys.* **2001**, *89*, 2958−2967.

(10) Lin, I. N.; Koizumi, S.; Yater, J.; Koeck, F. Diamond Electron Emission. *MRS Bull.* **2014**, *39*, 533−541.

(11) Chang, T. H.; Lou, S. C.; Chen, H. C.; Chen, C. L.; Lee, C. Y.; Tai, N. H.; Lin, I. N. Enhancing the Plasma Illumination Behaviour of Microplasma Devices using Microcrystalline/ Ultrananocrystalline Hybrid Diamond Materials as Cathodes. *Nanoscale* **2013**, *5*, 7467−7475.

(12) Sankaran, K. J.; Panda, K.; Sundaravel, B.; Chen, H. C.; Lin, I. N.; Lee, C. Y.; Tai, N. H. Engineering the Interface Characteristics of Ultrananocrystalline Diamond Films Grown on Au-Coated Si Substrates. *ACS Appl. Mater. Interfaces* **2012**, *4*, 4169−4176.

(13) Chen, H. C.; Sankaran, K. J.; Lou, S. C.; Lin, L. J.; Tai, N. H.; Lee, C. Y.; Lin, I. N. Using an Au Interlayer to Enhance Electron Field Emission Properties of Ultrananocrystalline Diamond Films. *J. Appl. Phys.* **2012**, *112*, No. 103711.

(14) Chang, T. H.; Panda, K.; Panigrahi, B. K.; Lou, S. C.; Chen, C.; Chan, H. C.; Lin, I. N.; Tai, N. H. Electrophoresis of Nanodiamond on the Growth of Ultrananocrystalline Diamond Films on Silicon Nanowires and the Enhancement of the Electron Field Emission Properties. *J. Phys.Chem. C* **2012**, *116*, 19867−19876.

(15) Nebel, C. E.; Yang, N.; Uetsuka, H.; Osawa, E.; Tokuda, N.; Williams, O.; Diamond Nano-Wires, A. New Approach Towards Next Generation Electrochemical Gene Sensor Platforms. *Diamond Relat. Mater.* **2009**, *18*, 910−917.

(16) Fowler, R. H.; Nordheim, L. Electron Emission in Intense Electric Fields. *Proc. R. Soc. London, Ser. A* **1928**, *119*, 173−181.

(17) Chang, T. H.; Kunuku, S.; Hong, Y. J.; Leou, K. C.; Yew, T. R.; Tai, N. H.; Lin, I. N. Enhancement on the Stability of Electron Field Emission Behavior and the Related Microplasma Devices of Carbon Nanotubes by Coating Diamond Films. *ACS Appl. Mater. Interfaces* **2014**, *6*, 11589−11597.

(18) Kunuku, S.; Sankaran, K. J.; Dong, C. L.; Tai, N. H.; Leou, K. C.; Lin, I. N. Development of Long Lifetime Cathode Materials for Microplasma Application. *RSC Adv.* **2014**, *4*, 47865−47875.

(19) Sun, Z.; Shi, J. R.; Tay, B. K.; Lau, S. P. UV Raman Characteristics of Nanocrystalline Diamond Films with Different Grain Size. *Diamond Relat. Mater.* **2000**, *9*, 1979−1983.

(20) Ferrari, A. C.; Robertson, J. Origin of the 1150−cm^{-1} Raman Mode in Nanocrystalline Diamond. *Phys. Rev. B* **2001**, *63*, No. 121405.

(21) Michler, J.; von Kaenel, Y.; Stiegler, J.; Blank, E. Complementary Application of Electron Microscopy and Micro-Raman Spectroscopy for Microstructure, Stress, and Bonding Defect Investigation of Heteroepitaxial Chemical Vapor Deposited Diamond Films. *J. Appl. Phys.* **1998**, *83*, 187−197.

(22) Lin, I. N.; Chen, H. C.; Wang, C. S.; Lee, Y. R.; Lee, C. Y. Nanocrystalline Diamond Microstructures from Ar/H_2/CH_4-Plasma Chemical Vapour Deposition. *CrystEngComm* **2011**, *13*, 6082−6089.

(23) Cheng, H. F.; Chiang, H. Y.; Horng, C. C.; Chen, H. C.; Wang, C. S.; Lin, I. N. Enhanced Electron Field Emission Properties by Tuning the Microstructure of Ultrananocrystalline Diamond Film. *J. Appl. Phys.* **2011**, *109*, No. 033711.

(24) Cheng, H. F.; Horng, C. C.; Chiang, H. Y.; Chen, H. C.; Lin, I. N. Modification on the Microstructure of Ultrananocrystalline Diamond Films for Enhancing Their Electron Field Emission Properties via a Two-Step Microwave Plasma Enhanced Chemical Vapor Deposition Process. *J. Phys. Chem. C* **2011**, *115*, 13894−13900.

(25) Wang, C. S.; Chen, H. C.; Cheng, H. F.; Lin, I. N. Synthesis of Diamond using Ultra-Nanocrystalline Diamonds as Seeding Layer and Their Electron Field Emission Properties. *Diamond Relat. Mater.* **2009**, *18*, 136−140.

(26) Chen, S. S.; Chen, H. C.; Wang, W. C.; Lee, C. Y.; Lin, I. N.; Guo, J.; Chang, C. L. Effects of High Energy Au-Ion Irradiation on the Microstructure of Diamond Films. *J. Appl. Phys.* **2013**, *113*, No. 113704.

(27) Kovarik, P.; Bourdon, E. B. D.; Prince, R. H. Electron-Energy-Loss Characterization of Laser-Deposited *a*-C, *a*-C:H, and Diamond Films. *Phys. Rev. B* **1993**, *48*, 12123−12129.

(28) Prawer, S.; Peng, J. L.; Orwa, J. O.; McCallum, J. C.; Jamieson, D. N.; Bursill, L. A. Size Dependence of Structural Stability in Nanocrystalline Diamond. *Phys. Rev. B* **2000**, *62*, 16360−16363.

DOI: 10.1021/acsami.5b00844
ACS Appl. Mater. Interfaces 2015, 7, 7732−7740